Smearing of quantum states and giant oscillations of the acoustoelectric current in a quantum channel

1997 J. Phys.: Condens. Matter 9 8381

(http://iopscience.iop.org/0953-8984/9/40/006)

J. Phys.: Condens. Matter **9** (1997) 8381–8395. Printed in the UK PII: S0953-8984(97)84001-5

Smearing of quantum states and giant oscillations of the acoustoelectric current in a quantum channel

Ø Lund Bø†, H Totland† and Yu Galperin†‡

† Department of Physics, University of Oslo, PO Box 1048, Blindern, N 0316 Oslo, Norway
‡ A F Ioffe Physico-Technical Institute, 194021 St Petersburg, Russia

Received 7 May 1997

Abstract. A quantum theory for the dc current induced by a surface acoustic wave (the acoustoelectric current) in a uniform quasi-one-dimensional quantum channel has been worked out. In long ballistic channels, giant oscillations of the acoustoelectric current were observed. According to the theoretical predictions (Gurevich *et al* 1996 *Phys. Rev. Lett.* **77** 3881), in a perfect uniform channel a finite acoustoelectric current exists only if the acoustic frequency exceeds the specific threshold value which is determined by the momentum and energy conservation laws. However, a finite current has been clearly observed well below the threshold. In the present paper, we show that electron scattering against a random short-range potential leads to an additional backscattering, as well as to a smearing of the momentum conservation law. As a result, a finite current appears well below the threshold acoustic frequency. The analysis is performed using the Keldysh non-equilibrium Green's function technique.

1. Introduction

The interaction between a surface acoustic wave (SAW) and a two-dimensional electron gas (2DEG) in mesoscopic conductors has gained considerable attention during the last few years.

One way to investigate the interaction is to observe its influence on the propagating acoustical wave. The transfer of energy and quasi-momentum from the SAW to the electron gas results in a sound attenuation, as well as in a renormalization of the sound velocity [1–5]. It is thus possible to investigate the response of a 2DEG to ac strains and, in the case of piezoelectric interaction, to ac electric fields, without contacts being attached to the sample.

Another method is to study the *acoustoelectric effect*, which is due to the SAW-induced electron drag [6–10]. In a closed electric circuit, the momentum transfer leads, in particular, to a dc current through the conductor which in the simplest situation is proportional to the SAW intensity. Alternatively, if the circuit is open, a dc voltage is induced across the sample.

Shilton *et al* [11] observed experimentally the acoustoelectric current through a *quasi-one-dimensional quantum channel* (figure 1) defined in a GaAs–AlGaAs heterostructure by a split-gate depletion technique. The channel clearly showed (the familiar) quantized conductance [12, 13] in units of $2e^2/h$. Contrary to what one might expect, the acoustoelectric current was not quantized, but showed instead *giant quantum oscillations* as a function of the gate voltage. The acoustoelectric current had maxima at the steps between the conductance plateaus.

0953-8984/97/408381+15$19.50

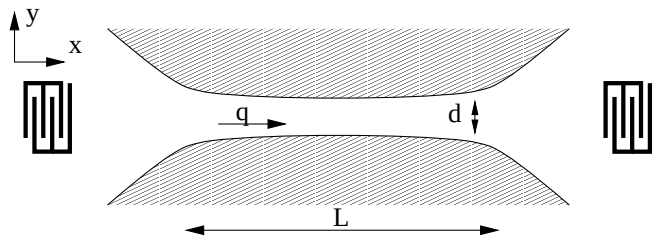

Figure 1. A schematic diagram of the experiment performed to measure the acoustoelectric current in a quantum wire.

The results [11, 14] were understood under the assumption that the major contribution to the SAW phonon drag on electrons takes place *inside* the quantum channel. In the case of a piezoelectric coupling, this assumption is justified, since the coupling is significantly screened in the wide regions (leads) because of the large conductance of the 2DEG. However, the screening is strongly suppressed inside the narrow 1D channel if its width is not much larger than the Bohr radius. Indeed, if the major interaction were taking place in the 2DEG reservoirs, a 'phonon wind' created in the leads would manifest itself as an additional electric field, leading to current *steps* [15].

The explanation suggested in references [11, 14] was based on the semi-classical Boltzmann equation. In parallel, a quantum theory for a perfect uniform channel has been developed [16]. As was shown in reference [16], the acoustoelectric current in a uniform ballistic channel has a cut-off at $q = q_{\rm th} \equiv 2m^*s/\hbar$, where $\boldsymbol{q}$ is the phonon wave vector, s is the sound velocity, and m^* is the effective electron mass. In the region where $q < q_{\rm th}$, corresponding to the condition $\omega < \omega_{\rm th} = 2m^*s^2/\hbar$ for the SAW frequency, *backscattering* is forbidden by the conservation laws. As a result, no acoustoelectric current is induced.

On the other hand, in the experiments [11, 17] the inequality $\omega < \omega_{\rm th}$ was met, but the oscillations were clearly observed. We believe that there are two reasons for the absence of a sharp cut-off, namely, (i) acoustically induced transitions between the propagating and reflecting modes near the edges of the channel, and (ii) impurity scattering inside the channel. The first reason was extensively discussed in connection with the photoconductance of ballistic channels [18], as well as in connection with the acoustoelectric effect [19] (see also below). The purpose of the present article is to work out a quantum theory of the acoustoelectric effect which allows for the finite relaxation rates originating from impurity scattering. The scattering against a short-range (in comparison to the channel's length) random impurity potential leads to an *electron level broadening* and, consequently, to a smearing of the conservation laws. This quantum effect overlaps the effect that can be allowed for within the framework of the Boltzmann-like equation, namely, an additional relaxation of the acoustically induced non-equilibrium electron distribution. In this paper, we focus on those effects in a uniform channel. To take account of both effects on an equal footing, the non-equilibrium Green's function formalism [20, 21] is appropriate.

2. The model

We consider a uniform quantum wire of length L (figure 1), parallel to the x-axis. The SAW also propagates along the x-axis. For convenience, the zero of the x-coordinate has been chosen to lie at the middle of the conductor. It is assumed that the coupling takes place only inside the channel.

The model of course needs few modifications to reproduce all of the details for realistic experimental systems.

First, there is still left a finite electron–SAW coupling in the leads. This coupling produces a 'phonon wind' for the electrons [15]. Consequently, finite current steps can appear, which overlap with the giant oscillations pattern originating from the intra-channel coupling. However, in the case of a *piezoelectric* coupling, the ac piezoelectric fields are significantly screened in the 2D leads in comparison with the quasi-1D wire region. Indeed, the screening length in a 2DEG is of the order of the Bohr radius $a_B = \epsilon\hbar^2/m^*e^2$, and if the dimensions of the 2D leads are much larger than a_B, then the interaction is effectively screened out. At the same time, the width of the wire might be comparable to a_B, in which case the electric field penetrates the channel, and the SAW–electron interaction inside the channel is much stronger than that in the leads. In this case, the current steps are weak compared to the giant oscillations.

Second, there is of course no abrupt drop in the effective coupling strength at the entrance and exit of the uniform 1D wire region. Rather, one can expect a smooth decrease of the effective coupling at the crossover between the 1DEG wire and the 2DEG leads. Important entrance and exit effects appear due to the finite coupling in those regions. In particular, the scattering of electrons between propagating and non-propagating modes in those regions may lead to additional oscillations in the acoustoelectric current [18, 19]. These effects are neglected in the present work. What we discuss is actually a model of a long, uniform quantum wire of length L, connecting two wide leads and subjected to a random impurity potential with a correlation length much less than L.

In the uniform wire model, the electronic states are described as products of wave functions which represent motion in longitudinal and transverse directions. The longitudinal motion (along the x-axis) is represented by plane waves with the wave vector k. The transverse motion (along the y-axis) is quantized, the mode being described by a discrete quantum number n. For convenience, we label the states by the quantum number $\alpha = (n, k)$. The electronic stationary states and the corresponding energy levels are thus

$$\begin{aligned} &\Psi_\alpha(\boldsymbol{r}) = L^{-1/2}\mathrm{e}^{\mathrm{i}kx}\chi_n(y) \\ &E_\alpha = E_n + E_k = E_n + \hbar^2k^2/2m^*. \end{aligned} \tag{1}$$

The actual form of E_n depends on the properties of the external potential which confines the electrons in the y-direction. The model Hamiltonian of the electron system is given by

$$\mathcal{H} = \mathcal{H}_{\mathrm{el}} + \mathcal{H}_{\mathrm{I}} = \mathcal{H}_{\mathrm{el}} + \mathcal{H}_{\mathrm{el-ph}} + \mathcal{H}_{\mathrm{el-i}} \tag{2}$$

with the unperturbed Hamiltonian

$$\mathcal{H}_{\mathrm{el}} = \sum_\alpha E_\alpha c_\alpha^\dagger c_\alpha \tag{3}$$

where $c_\alpha^\dagger$ (c_α) is the creation (annihilation) operator for an electron in the state α. Interaction with phonons and impurities is in this picture treated as a perturbation. The electron–phonon coupling is represented by [22]

$$\mathcal{H}_{\mathrm{el-ph}} = \sum_{\alpha,\beta,\boldsymbol{q}} W_{\alpha\beta}(\boldsymbol{q})(b_{\boldsymbol{q}} + b_{-\boldsymbol{q}}^\dagger)c_\alpha^\dagger c_\beta \tag{4}$$

where

$$W_{\alpha\beta}(\boldsymbol{q}) = w(\boldsymbol{q})\langle\alpha|\mathrm{e}^{\mathrm{i}\boldsymbol{q}\cdot\boldsymbol{r}}|\beta\rangle \tag{5}$$

is the electron–phonon interaction matrix, $w(\boldsymbol{q})$ is the coupling factor, which depends on the type of phonon, and $b_{\boldsymbol{q}}^\dagger$ ($b_{\boldsymbol{q}}$) is the creation (annihilation) operator for a phonon with wave vector $\boldsymbol{q}$.

In the case of piezoelectric interaction, the coupling factor is given by an expression of the type [23]

$$w(\boldsymbol{q}) = M_\lambda(\hat{\boldsymbol{q}})(\hbar/2\rho\mathcal{V}_0\omega_{\boldsymbol{q}})^{1/2} \tag{6}$$

where ρ is the mass density, $\mathcal{V}_0$ is the normalization volume, and $M_\lambda(\hat{\boldsymbol{q}})$ is the piezoelectric coupling tensor, which depends on the propagation direction $\hat{\boldsymbol{q}} \equiv \boldsymbol{q}/q$ and polarization λ of the phonons. In general, one has to sum over the phonon branches and wave vectors $\boldsymbol{q}$ in the Hamiltonian (4). In our problem, however, the propagating SAW has a definite constant polarization and direction. Consequently, the interaction tensor can be taken as a constant, $M_\lambda(\hat{\boldsymbol{q}}) \to M$, and (4) applies perfectly as our model Hamiltonian.

For the deformation potential coupling mechanism, the factor (6) has to be replaced by

$$w(\boldsymbol{q}) = D(\hbar\boldsymbol{q}^2/2\rho\mathcal{V}_0\omega_{\boldsymbol{q}})^{1/2} \tag{7}$$

where D is the deformation potential constant.

The frequency dependences of the piezoelectric and the deformation coupling mechanisms are different. For a relatively small SAW frequency ($\sim$3 GHz, as in the experiments in references [11, 17]), the piezoelectric interaction definitely dominates. However, for higher frequencies one can expect the deformational coupling to play an increasingly important role. In our further calculations we only consider the piezoelectric coupling.

The coupling to the random distributed impurities can be represented by the model Hamiltonian [22]

$$\mathcal{H}_1 = \frac{1}{\mathcal{V}_0}\sum_{\boldsymbol{q},\alpha,\beta,i} \mathrm{e}^{-\mathrm{i}\boldsymbol{q}\cdot\boldsymbol{R}_i} V_{\alpha\beta}(\boldsymbol{q}) c_\alpha^\dagger c_\beta \tag{8}$$

where $\boldsymbol{R}_i$ is the position of the ith impurity centre,

$$V_{\alpha\beta}(\boldsymbol{q}) = \langle\alpha|\mathrm{e}^{\mathrm{i}\boldsymbol{q}\cdot\boldsymbol{r}}|\beta\rangle = \int \mathrm{d}^3\boldsymbol{r}\ \mathrm{e}^{-\mathrm{i}\boldsymbol{q}\cdot\boldsymbol{r}} V(\boldsymbol{r}) \tag{9}$$

and $V(\boldsymbol{r})$ is the potential of one impurity situated at $\boldsymbol{r} = 0$.

In the calculation of quantum statistical averages, the averages are taken over the impurity centres' positions [24], as well as over the quantum states and the thermal distributions between the states. One should, however, keep in mind that in a very small mesoscopic device, it is possible that only a very few impurity centres are located inside the conductor. The electronic transport in the channel may then strongly depend on the exact configuration of those potentials. In this sense, the relatively long-range impurities act as a modification of the uniform channel geometry adopted as our initial model. Backscattering effects of the type discussed in reference [18] for the case of the entrance and the exit regions may therefore also be important inside the uniform wire. This type of modification is of course neglected in our model with a short-range random potential.

3. Theoretical analysis

To calculate the acoustoelectric current in the quantum wire when level broadening is taken into account, we apply the Keldysh non-equilibrium Green's function method. For our analysis, the triangular representation [21] is used, in which case the electron (G) and phonon (D) Green's functions, as well as the corresponding electron self-energy (Σ), are represented by 2×2 matrices of the type

$$\hat{F} = \begin{pmatrix} F_R & F_K \\ 0 & F_A \end{pmatrix}. \tag{10}$$

Here $F_{R,A,K}$ are the retarded, advanced, or so-called Keldysh electron (phonon) Green's components. In real space and time, the respective electron Green's functions are defined as [20, 21]

$$\begin{aligned} G_R(\xi_1|\xi_2) &= -\mathrm{i}\theta(t_1-t_2)\langle\{\hat{\Psi}(\xi_1),\hat{\Psi}^\dagger(\xi_2)\}_+\rangle \\ G_A(\xi_1|\xi_2) &= \mathrm{i}\theta(t_2-t_1)\langle\{\hat{\Psi}(\xi_1),\hat{\Psi}^\dagger(\xi_2)\}_+\rangle \\ G_K(\xi_1|\xi_2) &= -\mathrm{i}\langle\{\hat{\Psi}(\xi_1),\hat{\Psi}^\dagger(\xi_2)\}_+\rangle \end{aligned} \tag{11}$$

where $\xi_i \equiv (\boldsymbol{r}_i, t_i)$, $\hat{\Psi}(\boldsymbol{r}, t)$ are the electron field operators

$$\hat{\Psi}(\boldsymbol{r}_1, t) = \sum_\alpha \Psi(\boldsymbol{r}) c_\alpha(t) \tag{12}$$

while $\{\hat{A},\hat{B}\}_\pm = \hat{A}\hat{B} \pm \hat{B}\hat{A}$. The phonon Green's functions are defined in a similar way with the replacement of the electron field operators by the phonon ones:

$$\hat{\phi}(\boldsymbol{r}, t) = \frac{1}{\sqrt{\mathcal{V}_0}} \sum_{\boldsymbol{q}} \left[b_{\boldsymbol{q}}(t) + b^\dagger_{-\boldsymbol{q}}(t) \right] \mathrm{e}^{\mathrm{i}\boldsymbol{q}\cdot\boldsymbol{r}} \tag{13}$$

and the anti-commutators $\{\ \}_+$ by the commutators $\{\ \}_-$. We assume that the phonons have a linear dispersion, $\omega_{\boldsymbol{q}} = sq$, where s is the sound velocity.

Let us now change to a representation for the electron Green's functions which is convenient for our problem. First, we note that both the SAW and the electrons propagate along the x-direction. Consequently, the perpendicular motion is entirely described by the transverse wave functions $\chi_n(y)$. Secondly, we are interested in the stationary current under the conditions of a stationary phonon beam. Consequently, a Fourier transformation with respect to the time difference $t_1 - t_2$ can be performed. Third, we choose the Wigner representation to describe the motion in the x-direction, taking $X = (x_1 + x_2)/2$ as the centre-of-mass coordinate and $x = x_1 - x_2$ as the relative one. Finally, a Fourier transform with respect to x is performed, transforming the electron Green's functions to k-space. According to this new representation, the electron Green's functions are given by

$$\begin{aligned} \hat{G}(\alpha, X, \varepsilon) = \overline{h}^{-1} \int \mathrm{d}x\ \mathrm{d}y_1\ \mathrm{d}y_2\ \mathrm{d}t\ \mathrm{e}^{-\mathrm{i}kx + \mathrm{i}\varepsilon t/\overline{h}} \chi^*_n(y_1)\chi_n(y_2) \\ \times\ \hat{G}(X + x/2, y_1, t | X - x/2, y_2, 0). \end{aligned} \tag{14}$$

Phonons are not confined by the split-gate structure. For simplicity, we assume the phonons to be three dimensional and moving in a homogeneous space. In this space, the phonon Green's functions are dependent only on the differences $\boldsymbol{r} \equiv \boldsymbol{r}_1 - \boldsymbol{r}_2$ and $t \equiv t_1 - t_2$, and can be entirely described by the wave vector $\boldsymbol{q}$ and energy ε as

$$\hat{D}(\boldsymbol{q}, \varepsilon) = \overline{h}^{-1} \int \mathrm{d}^3\boldsymbol{r}\ \mathrm{d}t\ \mathrm{e}^{-\mathrm{i}\boldsymbol{q}\cdot\boldsymbol{r} + \mathrm{i}\varepsilon t/\overline{h}} \hat{D}(\boldsymbol{r}, t). \tag{15}$$

In the above representation for a system close to equilibrium, the electron and phonon Green's functions reduce to

$$\begin{aligned} G_R(\alpha, \varepsilon) &= G^*_A(\alpha, \varepsilon) = [\varepsilon - E_\alpha + \mu - \Sigma_R(\alpha, \varepsilon) + \mathrm{i}\delta]^{-1} \\ G_K(\alpha, X, \varepsilon) &= -\mathrm{i}[1 - 2f(X, \varepsilon)]A(\alpha, \varepsilon) \\ D_R(\boldsymbol{q}, \varepsilon) &= D^*_A(\boldsymbol{q}, \varepsilon) = \sum_\pm [\varepsilon \pm \overline{h}\omega_{\boldsymbol{q}} + \mathrm{i}\delta]^{-1} \\ D_K(\boldsymbol{q}, \varepsilon) &= -2\pi\mathrm{i} \sum_\pm \left[1 + 2N_{\pm\boldsymbol{q}}\right] \delta(\varepsilon \mp \overline{h}\omega_{\boldsymbol{q}}) \end{aligned} \tag{16}$$

where $A(\alpha,\varepsilon) = -2\,\mathrm{Im}\,G_R(\alpha,\varepsilon)$ is the spectral function for electrons, and μ is the chemical potential. In equilibrium, the electrons are distributed according to the Fermi–Dirac function, $f(X,\varepsilon) \to f_0(\varepsilon) = [\mathrm{e}^{(\varepsilon-\mu)/k_BT}+1]^{-1}$, while thermal phonons have the Planck distribution, $N_{\boldsymbol{q}} \to N_0(\hbar\omega_{\boldsymbol{q}}) = [\mathrm{e}^{\hbar\omega_q/k_BT}-1]^{-1}$.

In the non-equilibrium situation, the above distribution functions for electrons and phonons are of course modified. The retarded and advanced Green's functions preserve their form, while the kinetic properties are determined by the Keldysh Green's function. In our case of a SAW propagating along a uniform channel, the distribution of acoustical phonons can be described as

$$N_{\boldsymbol{q}} = N_0(\hbar\omega_{\boldsymbol{q}}) + \mathcal{N}\delta_{q,q_0} \qquad \mathcal{N} \equiv U\mathcal{V}_0/\hbar s^2 q_0 \tag{17}$$

where U is the SAW intensity and $\boldsymbol{q}_0 = (q_0, 0, 0)$ is the wave vector of the phonon beam. In the following, it is assumed that the temperature is low enough that the non-equilibrium phonons dominate, in which case

$$\mathcal{N} \gg 1, N_0(\hbar\omega_{\boldsymbol{q}_0}). \tag{18}$$

Consequently, thermal phonons are neglected, and only the second term of (17) enters the equations.

The electron Keldysh Green's function represents the dynamics of the electron system and is found from the kinetic equation. In the case of a weakly interacting, dilute system, the gradient approximation is used, and [21]

$$\frac{\partial G_0^{-1}}{\partial X}\frac{\partial G_K}{\partial k} - \frac{\partial G_0^{-1}}{\partial k}\frac{\partial G_K}{\partial X} = \Sigma_K A - \Gamma G_K \tag{19}$$

where $\Gamma = -2\,\mathrm{Im}\,\Sigma_R$ is the finite broadening of electronic excitations and, within the uniform channel, $G_0^{-1} = \varepsilon - \hbar^2k^2/2m^* - E_n + \mu$. The kinetic equation can thus be written in terms of the collision integral $I(X,\alpha,\varepsilon)$ as

$$\frac{\partial}{\partial X}G_K(X,\alpha,\varepsilon) = \frac{m^*}{\hbar^2 k} I(X,\alpha,\varepsilon) \tag{20}$$

$$I(X,\alpha,\varepsilon) = \Sigma_K(X,\alpha,\varepsilon)A(\alpha,\varepsilon) - \Gamma(\alpha,\varepsilon)G_K(X,\alpha,\varepsilon). \tag{21}$$

After the electron Keldysh Green's function has been derived from the differential equation (20), the electronic current in the channel is found from

$$I_{\mathrm{dc}} = \frac{\mathrm{i}e\hbar}{m}\sum_n \int \mathrm{d}k\ \mathrm{d}\varepsilon\ kG_K(X,\alpha,\varepsilon). \tag{22}$$

The electron self-energy, as well as the collision integral, can be divided into two parts originating from the electron–phonon interaction and the impurity scattering, respectively:

$$\begin{aligned} &\hat{\Sigma} = \hat{\Sigma}^{\mathrm{ph}} + \hat{\Sigma}^{\mathrm{imp}} \\ &I(X,\alpha,\varepsilon) = I^{\mathrm{ph}}(\alpha,\varepsilon) + I^{\mathrm{imp}}(X,\alpha,\varepsilon). \end{aligned} \tag{23}$$

Note that the impurity contribution to the collision integral depends on X, while for the phonon coupling this is not the case in the lowest-order approximation (see sections 3.1 and 3.2). In the following analysis, we restrict ourselves to the low-intensity case. Consequently, it is assumed that the system is driven slightly out of equilibrium, in which case we can write

$$G_K = G_K^{\mathrm{eq}} + \Delta G_K \qquad \Delta G_K(X,\alpha,\varepsilon) \ll G_K^{\mathrm{eq}}. \tag{24}$$

As will be demonstrated in section 3.2, the impurity collision integral in the linear-in-ΔG_K approximation can be written as

$$I^{\mathrm{imp}}(X,\alpha,\varepsilon) = -\Gamma^{\mathrm{imp}}(n,\varepsilon)\,\Delta G_K(X,\alpha,\varepsilon) \tag{25}$$

where $\Gamma^{\rm imp} \equiv -2\,{\rm Im}\,\Sigma_R^{\rm imp}$. The kinetic equation (20) then reduces to

$$\frac{\partial}{\partial X}\Delta G_K = \frac{m}{\hbar^2 k}\left[I^{\rm ph}(\alpha,\varepsilon) - \Gamma^{\rm imp}(n,\varepsilon)\,\Delta G_K\right], \tag{26}$$

with the general solution

$$\Delta G_K = \frac{I^{\rm ph}(\alpha,\varepsilon)}{\Gamma^{\rm imp}(n,\varepsilon)} + \chi(\alpha,\varepsilon){\rm e}^{-\Gamma^{\rm imp}(n,\varepsilon)X/\hbar^2 k} \tag{27}$$

where the function $\chi(\alpha,\varepsilon)$ must be found from the boundary conditions. At $X = -L/2$ ($X = L/2$), all the right-moving (left-moving) electrons with $k > 0$ ($k < 0$) originate from the left (right) reservoir and thus have an equilibrium distribution. Consequently the actual boundary conditions are

$$\begin{aligned} &\Delta G_K(X = -L/2, \alpha, \varepsilon) = 0 \qquad k > 0 \\ &\Delta G_K(X = L/2, \alpha, \varepsilon) = 0 \qquad k < 0 \end{aligned} \tag{28}$$

from which the function $\chi(\alpha,\varepsilon)$ is found. The time average of the current must be constant throughout the conductor, and so for symmetry reasons we choose to calculate it in the middle of the channel, where $X = 0$, and

$$\Delta G_K|_{X=0} = \frac{I^{\rm ph}}{\Gamma^{\rm imp}}(1 - {\rm e}^{-m\Gamma^{\rm imp}L/2\hbar p}). \tag{29}$$

The current can now finally be written as

$$\begin{aligned} &I_{\rm dc} = \frac{{\rm i}eL}{2\hbar}\int_0^\infty {\rm d}k \int_{-\infty}^{\infty} {\rm d}\varepsilon \sum_n \eta(\alpha,\varepsilon)\mathcal{J}^{\rm ph}(n,k) \\ &\mathcal{J}^{\rm ph}(n,k) \equiv \left[I^{\rm ph}(n,k,\varepsilon) - I^{\rm ph}(n,-k,\varepsilon)\right] \end{aligned} \tag{30}$$

where

$$\eta(\alpha,\varepsilon) \equiv \frac{2\hbar p}{Lm^*\Gamma^{\rm imp}(n,\varepsilon)}\left[1 - {\rm e}^{-Lm^*\Gamma^{\rm imp}(n,\varepsilon)/2\hbar p}\right] \tag{31}$$

is a damping factor due to the finite impurity relaxation rate. This damping can be expressed in terms of the effective mean free path in the one-dimensional channel $l_{\rm eff}(n,\varepsilon) = \hbar p/m^*\Gamma^{\rm imp}(n,\varepsilon)$ as

$$\eta = (2l_{\rm eff}/L)(1 - {\rm e}^{-L/2l_{\rm eff}}). \tag{32}$$

In the ballistic limit $l_{\rm eff} \gg L$, $\eta \to 1$ and there is no damping from impurity scattering, while in the opposite limit of strong relaxation, $l_{\rm eff} \ll L$, the damping goes as $2l_{\rm eff}/L$.

In the lowest Born approximation (see equation (45) below), $l_{\rm eff}$ is related to the 2D bulk mean free path, l_B, as $l_{\rm eff} = l_B(pd/2\hbar)$. In our system, the most important participating electrons belong to the upper transverse mode and have an energy close to the Fermi level. The longitudinal electron wave vector $k = p/\hbar$ of those electrons is small and is in fact of the order of the phonon wave vector. Thus the product $pl_{\rm eff}/\hbar$ can be much less than one, which leads to the inequality $l_{\rm eff} \ll l_B$. Consequently, even though the bulk mean free path may be comparable with L, the *effective mean free path* in the quantum wire can be less than L.

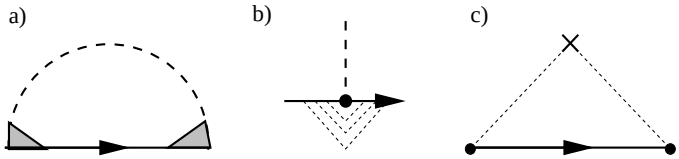

Figure 2. Feynman diagrams for (a) the lowest order in the electron–phonon contribution to the electron self-energy, (b) a typical diagram for impurity renormalization of the electron–phonon vertex, and (c) the impurity contribution to the self-energy in the first Born approximation.

3.1. Phonon self-energies and the collision integral

Formula (29) includes self-energies and collision integrals which are discussed in this section.

Let us start with the electron–phonon interaction. In the weakly interacting case of present interest, the self-energy is calculated to the lowest order according to the diagram in figure 2(a). The internal electron line in this diagram represents a Green's function which is dressed by impurity scattering. Using (18) and (24), we arrive at the following expression for the electron self-energies (appendix A):

$$\begin{aligned}\Sigma_R^{\rm ph}(\alpha,\varepsilon) &= \mathcal{N}\sum_{\beta,\pm}|\tilde{W}_{\alpha\beta}(\pm\boldsymbol{q}_0)|^2 G_R(\beta,\varepsilon_\mp)\\ \Sigma_K^{\rm ph}(\alpha,\varepsilon) &= -{\rm i}\mathcal{N}\sum_{\beta,\pm}\left[1-2f_0(\varepsilon_\mp)\right]|\tilde{W}_{\alpha\beta}(\pm\boldsymbol{q}_0)|^2 A(\beta,\varepsilon_\mp)\end{aligned} \tag{33}$$

where $\omega_0 \equiv \omega_{\boldsymbol{q}_0}$ is the SAW frequency, $\varepsilon_\pm \equiv \varepsilon \pm \hbar\omega_0$, while $\tilde{W}_{\alpha\beta}(\pm\boldsymbol{q}_0)$ is the electron–phonon vertex, renormalized by the impurities (it has the same matrix structure as the bare one because impurity scattering is elastic). The electron–phonon collision integral is then found from (21) and (33) as

$$I_{\rm ph}(\alpha,\varepsilon) = -{\rm i}\,2\mathcal{N}A(\alpha,\varepsilon)\sum_{\beta,\pm}\left[f_0(\varepsilon)-f_0(\varepsilon_\mp)\right]|\tilde{W}_{\alpha\beta}(\pm\boldsymbol{q}_0)|^2 A(\beta,\varepsilon_\mp). \tag{34}$$

The electron–phonon coupling matrix $\tilde{W}_{\alpha\beta}(\boldsymbol{q}_0)$, appearing in (33) and (34), includes the matrix elements

$$\langle\alpha|{\rm e}^{{\rm i}\boldsymbol{q}_0\cdot\boldsymbol{r}}|\beta\rangle = \frac{1}{L}\int {\rm d}^3\boldsymbol{r}\ |\varphi(z)|^2\chi_n^*(y)\chi_m(y){\rm e}^{{\rm i}(p-k)x}{\rm e}^{{\rm i}\boldsymbol{q}_0\cdot\boldsymbol{r}} \tag{35}$$

where $\alpha = (n,k)$, $\beta = (m,p)$, and $\varphi(z)$ is the part of the electron wave function confining the motion in the z-direction. Since $\boldsymbol{q}_0 = (q_0,0,0)$, the integration over the yz-plane leads to the conservation of the quantum channel index. In principle, the x-integration should be performed over the whole conductor, not only in the uniform wire, and so the x-dependence of k or p should be taken into account appropriately. Such a treatment would lead to a finite smearing of delta-functions for momentum conservation. In the experiments of reference [11], the channel was actually a quantum point contact which was shorter than the phonon wavelength. Therefore, the smearing should be taken into account in a corresponding theory. In our model, on the other hand, we assume for simplicity that the phonon wavelength is much smaller than the length of the uniform channel, $q_0L \gg 1$. Consequently, the matrix elements are approximated as

$$\langle\alpha|{\rm e}^{{\rm i}\boldsymbol{q}_0\cdot\boldsymbol{r}}|\beta\rangle \approx \delta_{m,n}\delta_{p,k-q_0}. \tag{36}$$

The renormalization of the electron–phonon vertex by impurity scattering (figure 2(b)) is known to be unimportant at $ql_{\rm eff} \gg 1$. This is the case for the energy range far enough

from the maximum in the acoustoelectric current. However, the velocities of the electrons responsible for the maxima of acoustoelectric current are small, and the above-mentioned condition can be violated. On the other hand, at $p/\hbar \gg l_{\rm eff}^{-1} \gg q$,

$$\tilde{W}_{\alpha\beta}(\boldsymbol{q}) \approx W_{\alpha\beta}(\boldsymbol{q}) \frac{\mathcal{D}q^2}{\mathcal{D}q^2 - \mathrm{i}\omega} \tag{37}$$

where $\mathcal{D} = v^2\tau_{\rm eff}$ is the diffusion constant for the electrons with the velocity v [25]. In the vicinities of the maxima the inequality $pl_{\rm eff} \gg \hbar$ is also not fulfilled, so there is no simple expression for the renormalized matrix elements. However, we will use equation (37) as an interpolation formula in the illustrative numerical calculations (see below).

Substituting the matrix elements (37) into (34), the phonon collision integral can finally be written as

$$I^{\rm ph}(n,k,\varepsilon) = -\mathrm{i}\,2\mathcal{N}|w(q_0)|^2 \frac{\mathcal{D}^2 q_0^4}{\mathcal{D}^2 q_0^4 + \omega_0^2} A(n,k,\varepsilon) \sum_{\pm} \left[f_0(\varepsilon) - f_0(\varepsilon_\pm) \right] A(n,k_\pm,\varepsilon_\pm) \tag{38}$$

where $k_\pm \equiv k \pm q_0$.

3.2. Impurity self-energies and the collision integral

Let us turn to the electron–impurity interaction. In the first Born approximation, corresponding to the diagram in figure 2(c),

$$\hat{\Sigma}^{\rm imp}(\alpha,\varepsilon) = \frac{n_i}{\mathcal{V}_0} \sum_{\beta,\boldsymbol{q}} |V_{\alpha\beta}(\boldsymbol{q})|^2 \hat{G}_0(\beta,\varepsilon) \tag{39}$$

where n_i is the density of impurities. In the following we assume that the scattering potential has a short correlation length compared to the channel length L. This is a necessary assumption for the impurity average technique to be adequate (otherwise the impurities should instead be taken into account as a modification of the channel geometry). At the same time we assume that the range is comparable with (or greater than) the channel width. This leads to the conservation of the channel index during transport and is thus a necessary condition for a pronounced quantization of conductance to be observed. As a consequence, the matrix element $V_{\alpha\beta}(\boldsymbol{q})$ is independent of $\boldsymbol{q}$ and can be written as

$$V_{\alpha\beta}(\boldsymbol{q}) = V\delta_{nm}. \tag{40}$$

Equation (39) can now be expressed in terms of the bulk 2DEG momentum relaxation time τ_B as

$$\hat{\Sigma}^{\rm imp}(n,\varepsilon) = \frac{\hbar}{\tau_B} \frac{\hbar^2}{2\pi m^* d} \int_{-\infty}^{\infty} \mathrm{d}k\ \hat{G}_0(n,k,\varepsilon) \tag{41}$$

where d is the channel width.

The impurity self-energy is important in two different ways in our equations—as a finite broadening of electronic excitations and as a relaxation mechanism expressed through the impurity collision integral. The finite broadening appears in the electron Green's functions and in the spectral functions that are included in the collision integrals and also in the expression for the current.

In the calculation of the acoustoelectric current, the relevant momentum for participating electrons is very small, in fact comparable with the phonon momentum. Consequently, we are operating very close to the one-dimensional singularities in the density-of-states (1D-DOS) function, and the perturbation approach that we employ fails. A simple but rather

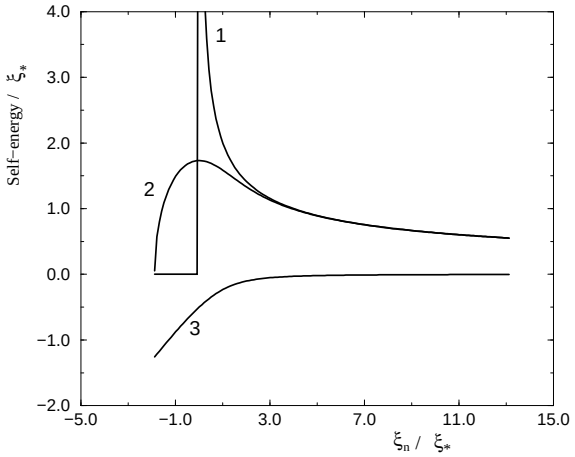

Figure 3. $\Gamma = -2\,\mathrm{Im}\,\Sigma$ and the real part $\mathrm{Re}\,\Sigma$ of the impurity-induced self-energy as functions of $\xi_n \equiv \varepsilon - E_n + \mu$. All of the energies are measured in units of ξ_*. Curve 1 is the escape rate Γ in the lowest Born approximation according to (45). Curves 2 and 3 show the corresponding escape rate and real part of the self-energy that result from the self-consistent equation (42).

effective way to treat the problem is to use the so-called self-consistent Born approximation [26], i.e. to make the replacement $\hat{G}_0 \rightarrow \hat{G}$ in equation (41) and then solve it self-consistently. Such an approach, though neglecting the vertex corrections, yields good numerical results for the spectral function. By the residue theorem we get

$$\Sigma_R^{\mathrm{imp}}(n,\varepsilon) = \mathrm{i}\,\mathrm{sgn}[\mathrm{Im}\,\Sigma_R^{\mathrm{imp}}(n,\varepsilon)]\frac{\xi_*^{3/2}}{\sqrt{\xi_n - \Sigma_R^{\mathrm{imp}}(n,\varepsilon)}}$$

with $\xi_n \equiv \varepsilon - E_n + \mu$ and $\xi_* \equiv (\hbar^2/\tau_B d\sqrt{2m})^{2/3}$. This means that $\Sigma_R^{\mathrm{imp}}(n,\varepsilon)$ is given as the complex solution with negative imaginary part of the third-order equation

$$z^3 - \xi_n z^2 - \xi_*^3 = 0. \tag{42}$$

The resulting $\Gamma^{\mathrm{imp}}(n,\varepsilon) \equiv -2\,\mathrm{Im}\,\Sigma_R^{\mathrm{imp}}(n,\varepsilon)$ is used as the finite broadening of levels in our numerical calculations below (figure 3). At $\xi_n \ll \xi_*$ one obtains

$$\Gamma^{\mathrm{imp}}(n,\varepsilon) \equiv \Gamma_* = \xi_*\sqrt{3}. \tag{43}$$

From (21) and (41), the X-dependent collision integral for the impurity scattering is given by

$$\begin{aligned} I^{\mathrm{imp}}(X,n,k,\varepsilon) &= \frac{\xi_*^{3/2}\hbar}{\pi\sqrt{2m}}\int_{-\infty}^{\infty}\mathrm{d}p\ \left[\mathcal{F}(p,k) - \mathcal{F}(k,p)\right] \\ \mathcal{F}(p,k) &\equiv \Delta G_K(X,n,p,\varepsilon)\,A(n,k,\varepsilon). \end{aligned} \tag{44}$$

For our problem, $A(n,k,\varepsilon)$ is symmetric in k, while this is not the case for $\Delta G_K(X,n,k,\varepsilon)$. The dc current inducing ΔG_K must actually, according to (22), be nearly anti-symmetric in k. Consequently, the first term in (44) gives a small contribution compared with the second term, and, in the linear relaxation approximation, the first is dropped. The impurity collision integral thus reduces to (25).

As a first estimate in the further analytical discussion we take the simplest Lorentzian broadening corresponding to the lowest Born approximation, in which case

$$\Gamma^{\mathrm{imp}}(n,\varepsilon) = 2\xi_*^{3/2}\xi_n^{-1/2}\Theta(\xi_n). \tag{45}$$

As demonstrated in figure 3, the lowest Born approximation is a good approximation provided that one is operating far beyond the 1D-DOS singularity, when $\xi_n > 3\xi_*$. Close to the singularity, on the other hand, there is a significant deviation between the lowest and the self-consistent Born approximations.

4. The case of negligible level broadening

Let us, in a first estimate, neglect the finite broadening of electronic levels, in which case all spectral functions are treated as delta-functions, $A(\alpha,\varepsilon) \to 2\pi\delta(\varepsilon - E_\alpha + \mu)$, and the energy can be easily integrated out of the expression for the current (30). Substituting the phonon collision integral (38) and integrating out the energy ε, we obtain

$$\begin{aligned} I_{\mathrm{dc}} = 4\pi^2\overline{h}^{-1}eL\mathcal{N}|w(\boldsymbol{q}_0)|^2 \sum_n \int_0^\infty \mathrm{d}k\ \eta(n,k,E_k-\mu) \\ \times \{[f_k^0 - f_{k-q_0}^0]\delta(E_{n,k} - \overline{h}\omega_0 - E_{n,k-q_0}) \\ + [f_k^0 - f_{k+q_0}^0]\delta(E_{n,k} + \overline{h}\omega_0 - E_{n,k+q_0}) \\ - [f_k^0 - f_{k+q_0}^0]\delta(E_{n,k} - \overline{h}\omega_0 - E_{n,k+q_0}) \\ - [f_k^0 - f_{k-q_0}^0]\delta(E_{n,k} + \overline{h}\omega_0 - E_{n,k-q_0})\} \end{aligned} \tag{46}$$

where $f_k^0 \equiv f_0(E_{n,k})$.

The delta-functions of energy appearing in (46) are transformed into delta-functions with respect to k as

$$\begin{aligned} &\delta(E_{n,k} - E_{n,k\pm q_0} \pm \overline{h}\omega_0) = (m^*/\overline{h}^2 q_0)\delta(k \pm k^\pm) \\ &k^\pm \equiv (q_0/2) \pm (m^* s/\overline{h}). \end{aligned} \tag{47}$$

Substituting those relations into (46) and integrating out the k-variable, in the case of piezoelectric interaction (6) we finally obtain the following simple expression for the acoustoelectric current:

$$I_{\mathrm{dc}} = (I_0/2)(f_{k^+}^0 - f_{k^-}^0)\sum_{\pm}\theta(\pm k^-)(\eta_+ \pm \eta_-) \tag{48}$$

where $\eta_\pm \equiv \eta(n, k^\pm, E_{n,k^\pm} - \mu)$, while

$$I_0 \equiv 2\pi^2 eLm^* UM^2/\rho\overline{h}^3\omega_0^3 \tag{49}$$

is the peak current in a ballistic channel (see below).

Since l_{eff} strongly depends on the electron velocity, when the relaxation from impurity scattering is significant, a finite current persists for $k^- < 0$, corresponding to $\omega < \omega_{\mathrm{th}}$. Indeed, since the velocity of participating electrons is very small and so $l_{\mathrm{eff}} \ll l_B$, the channel should be relatively short and extremely clean to observe any sign of a cut-off. As a first approximation, the condition for suppression of the subthreshold current reads

$$\frac{l_{\mathrm{eff}}}{L} \sim \frac{m^* s^2 \tau_B d}{2L\overline{h}} > 1. \tag{50}$$

The dependencies of the peak current on the quasi-Fermi level for three different values of the bulk relaxation time and $L = 0.5\ \mu$m are shown in figure 4. For $\tau_B = 10^{-10}$ s, there are

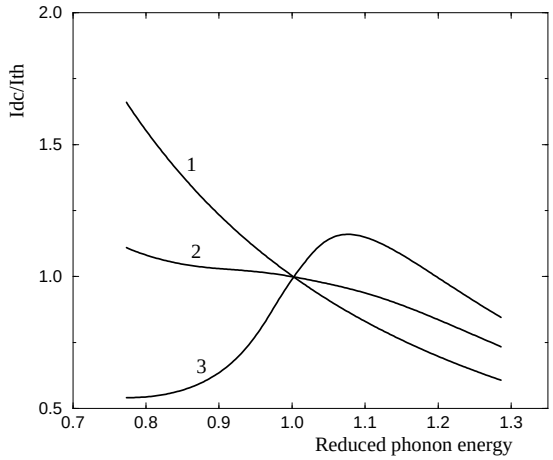

Figure 4. The peak value of the phonon-induced current as a function of the reduced phonon energy $\omega_q/\omega_{\rm th}$, where $\omega_{\rm th} = 2m^*s^2/\hbar$ is the threshold value. Three different cases are shown: curves 1, 2, and 3 correspond to $\tau_B\omega_{\rm th} = 2.95$, 29.5, and 147.5, respectively. The current is measured in units of the threshold current peak. All of the curves are for a channel of length $L = 0.5$ μm and $d \sim 80$ nm.

no signs of a cut-off. At $\tau_B = 10^{-9}$ s a weak structure appears, while at $\tau_B = 5 \times 10^{-9}$ s one can clearly observe suppression of the subthreshold current.

There are two different limiting cases which are particularly interesting. The first one is described by the inequality $l_{\rm eff} \ll L$, i.e. the case of a significant scattering by the short-range potential. In this case the estimates for the current peak below and above the threshold ($\omega_{\rm th}$) are of the same order. The current is proportional to τ_B and is L-independent. Within the lowest Born approximation,

$$I_{\rm dc} \approx \frac{I_0 d\tau_B}{L\omega_{\rm th}}\left[f^0_{k^+} - f^0_{k^-}\right]\begin{cases}\dfrac{1}{2}(\omega_0^2+\omega_{\rm th}^2) & \omega_0 \geqslant \omega_{\rm th}\\ \omega_0\omega_{\rm th} & \omega_0 < \omega_{\rm th}.\end{cases} \tag{51}$$

This result basically agrees with the one obtained in reference [14] with the help of the Boltzmann equation. In the self-consistent Born approximation the energy dependence of η is reduced, and the subthreshold current is consequently reduced as compared with the above-threshold case.

The second limit is $l_{\rm eff} \gg L$. In this case the current above the threshold is simply

$$I_{\rm dc} \approx I_0\left[f^0_{k^+} - f^0_{k^-}\right]. \tag{52}$$

This is the same result as was obtained for a uniform ballistic channel in reference [16]. The subthreshold current, in contrast, is in this case *inversely proportional* to τ_B and proportional to L^2:

$$I_{\rm dc} \approx \frac{I_0 L\omega_{\rm th}}{d\tau_B}\,\frac{\omega_0\omega_{\rm th}}{[\omega_0^2-\omega_{\rm th}^2]^2}\left[f^0_{k^+} - f^0_{k^-}\right]. \tag{53}$$

The result agrees with the estimate in reference [27] obtained for the case where $L \gg l_B$. The above formula has a singularity at $\omega_0 = \omega_{\rm th}$. Close to this threshold value, the expression is not valid, since $l_{\rm eff} \propto p/\hbar$, and so the initial assumption $|k^-l_{\rm eff}| \gg 1$, which was used in the series expansion of η, breaks down.

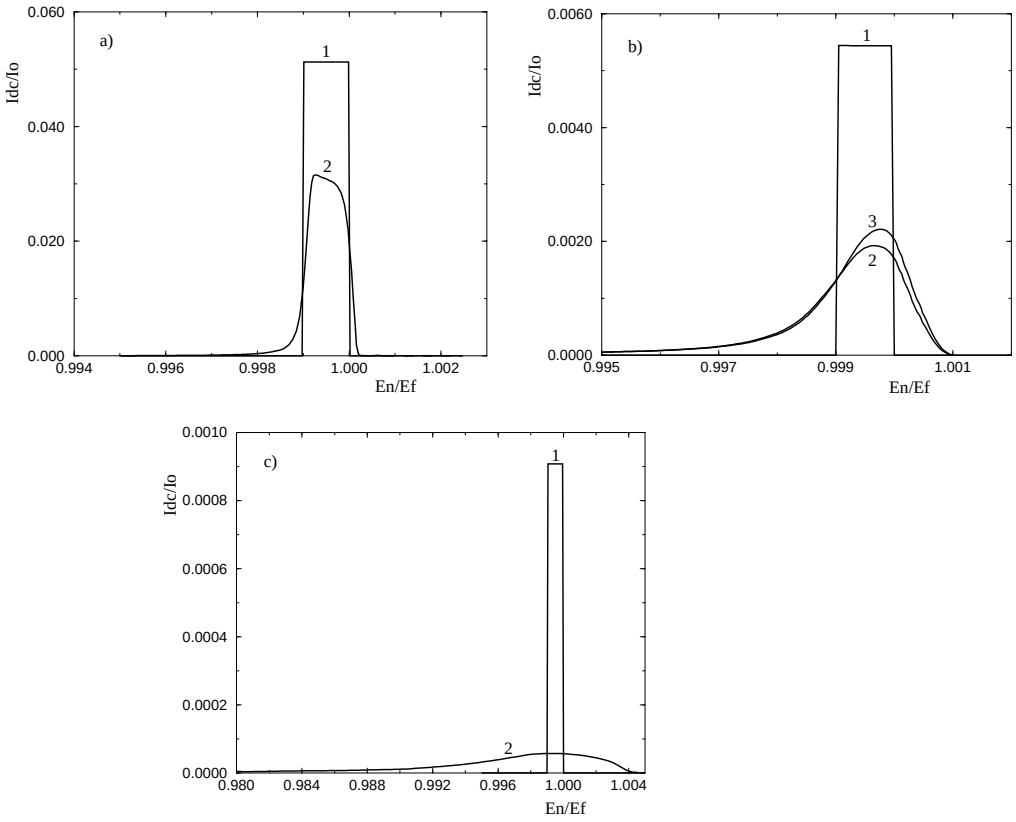

Figure 5. The acoustoelectric current as a function of the reduced transverse energy E_n/E_f (monitored by the gate voltage). Panels (a), (b), and (c) correspond to $\tau_B = 10^{-8}$ s ($\omega_{\rm th}\tau_B = 295$), 10^{-9} s (29.5), and 10^{-10} s (2.95), respectively. The current is plotted in units $I_0 \equiv 2\pi^2 eLm^*UM^2/\rho\bar{h}^3\omega_0^3$. The curves 1 are the results from the semi-classical model (48) while curves 2 are the quantum mechanical results including both the level broadening and the vertex corrections. In panel (b) we also demonstrate the role of vertex corrections by means of curve 3, which represents the current calculated without those corrections.

5. The effect of level broadening

In figure 5 we have plotted the results of the quantum mechanical numerical calculations of (30), where the effect of level broadening and renormalization of the electron–phonon vertices are taken into account. The curves show the acoustoelectric current as a function of transverse energy E_n. In real experiments, E_n is directly controlled by the gate voltage, and consequently the curves give a picture of $I_{\rm dc}$ versus gate voltage for our model system. At zero temperature, a phonon-induced current arises when the level E_n is within a layer of width $\bar{h}\omega_0$ around the Fermi level. Three different cases are considered, corresponding to $\tau_B = 10^{-10}$, 10^{-9}, and 10^{-8} s, and the calculated acoustoelectric current is compared with the corresponding classical result (48).

The level broadening has the effect that the current peak is clearly smeared out, and its maximum is significantly reduced in the strongly interacting case. As is demonstrated by means of one of the curves, the impurity renormalization of electron–phonon vertices leads to an additional, relatively small reduction of the peak current.

6. Conclusions

In conclusion, we have shown that the acoustoelectric current in a quasi-one-dimensional quantum channel is extremely sensitive to the scattering from random impurity centres inside the channel. The very low electron velocity of participating electrons is responsible for the fact that the effective mean free path is much less than the bulk mean free path in this problem. Consequently, any sign of a current threshold at the phonon frequency threshold value $\omega_{\rm th} = q_0 s = 2m^* s^2/\hbar$, as in a uniform ballistic channel, is only expected for extremely clean and short channels. The profile of the quantum oscillations of the acoustoelectric current is also very sensitive to the level broadening. The peaks are damped and smeared out because of this quantum effect.

Acknowledgments

We are grateful to V L Gurevich, V I Kozub, and V B Pevzner for making available a preprint of reference [27]. Two of us (ØLB and HT) are also grateful to the Norwegian Research Council for financial support.

Appendix A. The electron–phonon self-energy

In the triangular representation (10), the (i, j)-component of the first-order electron–phonon self-energy matrix, as represented by the diagram in figure 2(a), is given by [21]

$$\hat{\Sigma}^{\rm ph}_{ij}(\alpha, \varepsilon) = {\rm i}\sum_{\boldsymbol{q},\beta} |W_{\alpha\beta}(\boldsymbol{q})|^2 \int \frac{{\rm d}\varepsilon_1}{2\pi} \sum_{i',j',l,l'} \mathcal{T}^l_{ii'} \hat{G}_{i'j'}(\beta, \varepsilon - \varepsilon_1) \hat{D}_{ll'}(\boldsymbol{q}, \varepsilon_1) \tilde{\mathcal{T}}^{l'}_{j'j} \tag{A1}$$

where $\mathcal{T}^l_{ii'}(\alpha, \beta, \varepsilon - \varepsilon_1)$ is the impurity-induced contribution to the vertex part. In the case of elastic scattering from static impurities, the Keldysh matrix structure is conserved and $\mathcal{T}^l_{ii'}(\alpha, \beta, \varepsilon - \varepsilon_1) \propto \gamma^l_{ii'}$ where $\gamma^1_{ij} = \tilde{\gamma}^2_{ij} = 2^{-1/2}\delta_{ij}$, $\gamma^2_{ij} = \tilde{\gamma}^1_{ij} 2^{-1/2}\sigma^x_{ij}$, and σ^x is the x-directed Pauli matrix. Having in mind the fact that we are interested only in the contribution of *real* non-equilibrium phonons in the lowest order in the electron–phonon interaction, we can absorb $\mathcal{T}^l_{ii'}(\alpha, \beta, \omega_{\boldsymbol{q}})$ into the renormalized coupling constant $|\tilde{W}_{\alpha\beta}|^2$. With the substitution of the phonon Green's functions from (16) and integration over the internal energy ε_1, we arrive at

$$\Sigma^{\rm ph}_R(\alpha, \varepsilon) = \sum_{\boldsymbol{q},\beta} |\tilde{W}_{\alpha\beta}(\boldsymbol{q})|^2 \left\{ G_R(\beta, \varepsilon_-) \left[1 + N_{\boldsymbol{q}} - f(\varepsilon_-)\right] + G_R(\beta, \varepsilon_+) \left[N_{-\boldsymbol{q}} + f(\varepsilon_+)\right] \right\} \tag{A2a}$$

$$\Sigma^{\rm ph}_K(\alpha, \varepsilon) = -{\rm i}\sum_{\boldsymbol{q},\beta} |\tilde{W}_{\alpha\beta}(\boldsymbol{q})|^2 \left\{ A(\beta, \varepsilon_-) \left[1 + N_{\boldsymbol{q}} - f(\varepsilon_-) - 2N_{\boldsymbol{q}} f(\varepsilon_-)\right] + A(\beta, \varepsilon_+) \left[N_{-\boldsymbol{q}} - f(\varepsilon_+) - 2N_{-\boldsymbol{q}} f(\varepsilon_+)\right] \right\} \tag{A2b}$$

with $\varepsilon_\pm \equiv \varepsilon \pm \hbar\omega_{\boldsymbol{q}}$. Since the acoustically induced effects are determined by the *non-equilibrium* phonons, we can substitute $N_{\boldsymbol{q}} = \mathcal{N}\delta_{\boldsymbol{q},\boldsymbol{q}_0}$. In this way we arrive at (33).

References

[1] Wixforth A, Kotthaus J P and Weinman G 1986 *Phys. Rev. Lett.* **56** 2104
[2] Wixforth A, Scriba J, Wassermeier M, Kotthaus J P, Weinman G and Schlapp W 1998 *Phys. Rev.* B **40** 7874
[3] Willett R L, Palaanen M A, Ruel R R, West K W, Pfeiffer L N and Bishop D J 1990 *Phys. Rev. Lett.* **65** 112
[4] Willett R L, Ruel R R, West K W and Pfeiffer L N 1993 *Phys. Rev. Lett.* **71** 3846

[5] Rodrigues C, Fonzeca A L A and Nunes O A C, 1995 *Phys. Status Solidi* b **189** 117
[6] Efros A L and Galperin Yu M 1990 *Phys. Rev. Lett.* **64** 1959
[7] Esslinger A, Wixforth A, Winkler R W, Kotthaus J P, Nickel H, Schlapp W and Losch L 1992 *Solid State Commun.* **84** 949
[8] Falko V I, Meshkov S V and Iordanski S V 1993 *Phys. Rev.* B **47** 9910
[9] Shilton J M, Mace D R, Talyanskii V I, Pepper M, Simmons M Y, Churchill A C and Ritchie D A 1995 *Phys. Rev.* B **51** 14 770
[10] Shilton J M, Mace D R, Talyanskii V I, Simmons M Y, Pepper M, Churchill A C and Ritchie D A 1995 *J. Phys.: Condens. Matter* **7** 7675
[11] Shilton J M, Mace D R, Talyanskii V I, Galperin Yu M, Simmons M Y, Pepper M and Ritchie D A 1996 *J. Phys.: Condens. Matter* **8** L337
[12] van Wees B J, van Houten H, Beenakker C W J, Williamson J G, Kouwenhoven L P, van der Marel D and Foxon C 1988 *Phys. Rev. Lett.* **60** 848
[13] Wharam D A, Thornton T J, Newbury R, Pepper M, Ahmed H, Frost J E F, Hasko D G, Peacock D G, Ritchie D A and Jones G A C 1988 *J. Phys. C: Solid State Phys.* **21** L209
[14] Totland H and Galperin Y 1996 *Phys. Rev.* B **54** 8814
[15] Kozub V I and Rudin A M 1994 *Phys. Rev.* B **50** 2681
[16] Gurevich V L, Pevzner V B and Iafrate G J 1996 *Phys. Rev. Lett.* **77** 3881
[17] Shilton J M, Talyanskii V I, Pepper M, Ritchie D A, Frost J E F, Ford C J B, Smith C G and Jones G A C 1996 *J. Phys.: Condens. Matter* **8** L531
[18] Grincwajg A, Gorelik L Y, Kleiner V Z and Shekter R I 1995 *Phys. Rev.* B **52** 12 168
Maaø F A and Gorelik L Y 1996 *Phys. Rev.* B **53** 15 885
[19] Maaø F A and Galperin 1997 *Phys. Rev.* B **56** 3517
[20] Keldysh L V 1964 *Zh. Eskp. Teor. Fiz.* **47** 1515 (Engl Transl. 1965 *Sov. Phys.–JETP* **20** 1018)
[21] Rammer J and Smith H 1986 *Rev. Mod. Phys.* **58** 323
[22] Mahan G D 1990, 1981 *Many-Particle Physics* (New York: Plenum)
[23] Mahan G D 1972 *Polarons in Ionic Crystals and Polar Semiconductors* ed J T Devreese (Amsterdam: North-Holland)
[24] Kohn W and Luttinger J M 1957 *Phys. Rev.* B **108** 590
[25] Altshuler B L and Aronov A G 1985 *Electron–electron Interactions in Disordered Systems* ed A L Efros and P Pollak (Amsterdam: North-Holland)
[26] Ando T, Fowler A B and Stern F 1982 *Rev. Mod. Phys.* **54** 437
[27] Gurevich V L, Kozub V I and Pevzner V B 1997 unpublished